# The Anglo-Australian Planet Search XXV: A Candidate Massive Saturn Analog Orbiting HD 30177

Robert A. Wittenmyer[1,2], Jonathan Horner[1,2], M.W. Mengel[1], R.P. Butler[3], D.J. Wright[2], C.G. Tinney[2], B.D. Carter[1], H.R.A. Jones[4], G. Anglada-Escudé[5], J. Bailey[2], Simon J. O'Toole[6]

rob@unsw.edu.au

## ABSTRACT

We report the discovery of a second long-period giant planet orbiting HD 30177, a star previously known to host a massive Jupiter analog (HD 30177b: a=3.8±0.1 au, m sin $i$ = 9.7±0.5 $M_{\rm Jup}$). HD 30177c can be regarded as a massive Saturn analog in this system, with a=9.9±1.0 au and m sin $i$ = 7.6±3.1 $M_{\rm Jup}$. The formal best fit solution slightly favours a closer-in planet at $a \sim 7$ au, but detailed $n$-body dynamical simulations show that configuration to be unstable. A shallow local minimum of longer-period, lower-eccentricity solutions was found to be dynamically stable, and hence we adopt the longer period in this work. The proposed ~32 year orbit remains incomplete; further monitoring of this and other stars is necessary to reveal the population of distant gas giant planets with orbital separations $a \sim 10$ au, analogous to that of Saturn.

*Subject headings:* planetary systems — techniques: radial velocities – stars: individual (HD 30177)

[1]Computational Engineering and Science Research Centre, University of Southern Queensland, Toowoomba, Queensland 4350, Australia

[2]School of Physics and Australian Centre for Astrobiology, University of New South Wales, Sydney 2052, Australia

[3]Department of Terrestrial Magnetism, Carnegie Institution of Washington, 5241 Broad Branch Road, NW, Washington, DC 20015-1305, USA

[4]Centre for Astrophysics Research, University of Hertfordshire, College Lane, Hatfield, Herts AL10 9AB, UK

[5]School of Physics and Astronomy, Queen Mary University of London, 327 Mile End Road, London E1 4NS, UK

[6]Australian Astronomical Observatory, PO Box 915, North Ryde, NSW 1670, Australia

# 1. Introduction

Prior to the dawn of the exoplanet era, it was thought that planetary systems around other stars would likely resemble our own - with small, rocky planets close to their host stars, and the more massive, giant planets at greater distances. With the discovery of the first exoplanets, however, that paradigm was shattered - and it rapidly became clear that many planetary systems are dramatically different to our own. But to truly understand how unusual (or typical) the Solar system is, we must find true Jupiter and Saturn analogs: massive planets on decade-long orbits around their hosts. The only way to find such planets is to monitor stars on decade-long timescales, searching for the telltale motion that might reveal such distant neighbours.

Nearly three decades of planet search have resulted in a great unveiling, at every stage of which we are finding our expectations consistently upturned as the true diversity of worlds becomes ever more apparent. Much progress has been made in understanding the occurrence rates and properties of planets orbiting within $\sim$1 au of their stars, brought on by the *Kepler* revolution (e.g. Borucki et al. 2011; Rowe et al. 2014; Coughlin et al. 2016) and the advent of Doppler velocimetry at precisions of $1\,\mathrm{m\,s^{-1}}$ (Fischer et al. 2016). While *Kepler* has been hugely successful in exploring the frequency of planets close to their stars, such transit surveys are not suited to search for planetary systems like our own - with giant planets moving on orbits that take decades to complete. To understand the occurrence of such systems requires a different approach - radial velocity monitoring of individual stars on decadal timescales.

Sometimes overshadowed by the *Kepler* dicoveries, but equally important for a complete picture of planetary system properties, are the results from ongoing "legacy" Doppler surveys, which are now sensitive to giant planets in orbits approaching 20 years. Those surveys include, for example, the McDonald Observatory Planet Search (Robertson et al. 2012; Endl et al. 2016), the California Planet Search (Howard et al. 2010; Feng et al. 2015), the Anglo-Australian Planet Search (Tinney et al. 2001; Wittenmyer et al. 2011, 2014b), and the Geneva Planet Search (Marmier et al. 2013; Moutou et al. 2015).

The emerging picture is that the Solar System is not typical of planetary systems in the Solar neighbourhood. For example, super-Earths, planets with masses $\sim$3-10 $\mathrm{M_\oplus}$, are extremely common yet are completely absent from our Solar System. Jupiter-like planets in Jupiter-like orbits appear to be relatively uncommon, orbiting only about 6% of solar-type stars (Wittenmyer et al. 2016b).

Such a low incidence of true Solar system analogs is of particular interest in the context of astrobiology, and the search for truly Earth-like planets beyond the Solar system. In the Solar System, Jupiter has played a key role in the formation and evolution of the planetary

system - variously corralling, sculpting and destabilising the system's smaller bodies (and thereby likely contributing significantly to the introduction of volatiles, including water, to the early Earth). Over the system's more recent history, Jupiter has managed the flux of smaller objects towards the Earth, influencing (but not necessarily reducing) the frequency of impacts on the terrestrial planets. It has long been argued that the presence of a true Jupiter analog would be an important selection factor for an Earth-like planet to be truly habitable - although many recent studies have suggested that this might not be the case (e.g. Horner & Jones 2008; Horner et al. 2010; Horner & Jones 2010b; Lewis et al. 2013).

The Anglo-Australian Planet Search (AAPS) monitored ∼250 solar-type stars for 14 years. Of these, a subset of ∼120 stars continued to be observed for a further three years, with the primary aim of detecting Jupiter-mass planets in orbits $P > 10$yr (Wittenmyer et al. 2016b). The AAPS has delivered a consistent $3\,\mathrm{m\,s^{-1}}$ velocity precision since its inception, enabling the discovery of several Jupiter analogs (e.g. Jones et al. 2010; Wittenmyer et al. 2012a, 2014a).

This paper is organised as follows: Section 2 outlines the AAT and HARPS observations of HD 30177 and gives the stellar parameters. Section 3 describes the orbit-fitting procedures and gives the resulting planetary parameters for the HD 30177 system. In Section 4 we perform a detailed dynamical stability analysis of this system of massive planets. Then we give our conclusions in Section 5.

## 2.   Observational Data and Stellar Properties

HD 30177 is an old, Sun-like star, with a mass within 5% of Solar. It lies approximately 54.7 parsecs from the Sun, and has approximately twice Solar metallicity. The stellar parameters for HD 30177 can be found in Table 1. We have observed HD 30177 since the inception of the AAPS, gathering a total of 43 epochs spanning 17 years (Table 6). Precise radial velocities are derived using the standard iodine-cell technique to calibrate the instrumental point-spread function (Valenti et al. 1995; Butler et al. 1996). The velocities have a mean internal uncertainty of $3.9\pm1.2\,\mathrm{m\,s^{-1}}$.

HD 30177 has also been observed with the HARPS spectrograph on the ESO 3.6m telescope in La Silla. At this writing, 20 epochs spanning 11 years are publicly available at the ESO Archive. Velocities were derived using the HARPS-TERRA technique (Anglada-Escudé & Butler 2012), and are given in Table 6.

## 3.   Orbit Fitting and Results

The inner planet, HD 30177b was first announced in Tinney et al. (2003), with a relatively unconstrained period of 1620±800 days and m sin $i$ = 7.7±1.5 M$_{\rm Jup}$. Its orbit was updated in Butler et al. (2006) on the basis of observations that clearly spanned one full orbital period, to $P$ = 2770±100 days and m sin $i$ = 10.5±0.9 M$_{\rm Jup}$. We now present a further 10 years of AAT data, along with 11 years of concurrent HARPS data, to refine the orbit of this planet. As a result of this additional data, we now find that the single-planet fit exhibits significant residuals, suggesting the presence of a second, very long-period object in this system. We have added 6 m s$^{-1}$ of jitter in quadrature to both data sets; this brings the reduced $\chi^2$ close to 1 for two-planet models. A single-planet model now has a reduced $\chi^2$ of 7.1 and an rms of 17.3 m s$^{-1}$. As in our previous work (e.g. Tinney et al. 2011; Wittenmyer et al. 2013; Horner et al. 2014; Wittenmyer et al. 2016a), we have used a genetic algorithm to explore the parameter space for the outer planet, fitting a simultaneous two-Keplerian model that allows the outer planet to take on periods 4000-8000 days and eccentricities $e < 0.3$. The best fit from the genetic algorithm results was then used as a starting point for a two-Keplerian fit (downhill simplex minimisation) within the *Systemic Console* (Meschiari et al. 2009).

The results of these fits are given in Table 4. The precision with which the parameters for the inner planet are known are now improved by a factor of ten, or more, over the previously published values (Butler et al. 2006). The model fit for the inner planet is shown in Figure 1. The nominal best fit solution features a second planet, HD 30177c, with period of 6921±621 days and m sin $i$ = 3.0±0.3 M$_{\rm Jup}$. We present both a "best fit" and a "long period" solution in recognition of the fact that for an incomplete orbit, the period can be wildly unconstrained and allow for solutions with ever-longer periods by adjusting the eccentricity. Figure 2 shows the $\chi^2$ contours as a function of the outer planet's period and eccentricity, based on the results from the best-fit solution given in the left columns of Table 4. The best fit solution appears to be a shallow minimum in the $\chi^2$ space, with a secondary minimum at lower eccentricity and longer period ($P \sim$10000 days). We thus attempted a second fit, starting the orbital period of the outer planet at 10000 days to guide the *Systemic* simplex algorithm into the apparent secondary $\chi^2$ minimum seen in Figure 2. The results are given in the right columns of Table 4, labelled "long period." This fit results in an outer planet with period 11640±2432 days and m sin $i$ = 6.4±3.3 M$_{\rm Jup}$; the uncertainties are of course much larger since the available data only cover $\sim$60% of the orbital period. The best-fit and long-period solutions are plotted in Figure 3.

One might argue that the outer planet hypothesis relies heavily on the presumption of a velocity turnover in the first few epochs, in particular the point at BJD 2451119, which lies

about $30\,\mathrm{m\,s^{-1}}$ below the previous night's velocity. To check the effect of this potentially bad observation, we repeated the orbit fitting described above after removing that point. The results are given in Table 5, again expressed as a "best fit" and a "long period" solution. We now find a best fit at a period of $7601\pm1134$ days and m sin $i = 3.3\pm0.5\,\mathrm{M_{Jup}}$. Removing the suspected outlier resulted in a slightly longer period that remains in formal agreement with the original solution in Table 4. For the long-period solution, we again started the *Systemic* fitting routine at a period of 10,000 days for the outer planet. This results again in a long period consistent with the long period solution obtained from the full set of velocities: we obtain a period of $11613\pm1837$ days and m sin $i = 7.6\pm3.1\,\mathrm{M_{Jup}}$. We thus have two possible solutions for the HD 30177 two-planet system, which are virtually indistinguishable in terms of the RMS about the model fit or the $\chi^2$, due to the shallow minima and complex $\chi^2$ space (Figure 4).

For the old, solar-type stars generally targeted by radial velocity surveys, stellar magnetic cycles like the Sun's 11-year cycle are a concern when claiming detection of planets with orbital periods ∼10 years and longer. While our AAT/UCLES spectra do not include the Ca II H and K lines most commonly used as activity proxies, the HARPS spectra used in this work do (e.g. Dumusque et al. 2011; Lovis et al. 2011; Hébrard et al. 2014). Figure 5 shows the Ca II activity $\log R'_{HK}$ versus the HARPS radial velocities. No correlation is evident. Clearly, a long-period body is present, but a longer time baseline is necessary to observe a complete orbit and better constrain its true nature. In the next section, we explore the dynamical stability of the two candidate orbital solutions.

## 4. Dynamical Stability Simulations

In order to understand the dynamical context of the two distinct orbital solutions presented above, and to see whether they yield planetary systems that are dynamically feasible, we followed a now well-established route (e.g. Marshall et al. 2010; Robertson et al. 2012; Horner et al. 2013). For each solution, we performed 126,075 unique integrations of the system using the Hybrid integrator within the $n$-body dynamics package, MERCURY (Chambers 1999). In each of those simulations, we held the initial orbit of the innermost planet fixed at its nominal best-fit values (as detailed in Table 4). We then proceeded to systematically move the orbit of the outermost planet through the full $\pm3\sigma$ uncertainty ranges for semi-major axis, $a$, eccentricity, $e$, argument of periastron, $\omega$, and mean anomaly, $M$. In this manner, we created a regular grid of solutions, testing 41 unique values of $a$ and $e$, 15 unique values of $\omega$, and 5 unique values of $M$.

These simulations make two assumptions: first, that the two planets move on coplanar

orbits (as is essentially the case in the Solar system), and second, we assign the planets their minimum masses (m sin $i$) as derived from the radial velocity data. In a number of previous studies (e.g. Horner et al. 2011, 2014; Hinse et al. 2014), we have examined the impact of mutual inclination on system stability. However, for widely separated planets, the inclination between the two orbits seems to play little role in their stability. It seems most likely that there would not be large mutual inclination between the orbits of the planets; from a dynamical point of view, given the assumption that the two planets formed in a dynamically cool disk, it is challenging to imagine how they could achieve significant mutual inclination without invoking the presence of a highly inclined distant perturber (i.e. an undetected binary companion, driving excitation through the Kozai mechanism). It is certainly reasonable to assume that the orbits are most likely relatively coplanar, as is seen in the Solar system giant planets, and also in those multiple exoplanet systems with orbital inclinations constrained by transits (Fang & Margot 2012) or by resolved debris disk observations (Kennedy et al. 2013).

Regarding the use of minimum masses, one would expect increased planetary masses to destabilise the systems. The reason for this can be seen when one considers the "gravitational reach" of a planet, which can be defined in terms of its Hill radius. The Hill radius is proportional to the semi-major axis of the planet's orbit, but only increases as the cube root of the planet's mass. As a result, doubling the mass of a planet only increases its gravitational reach, and therefore its Hill radius, by a factor of $2^{(1/3)} = 1.26$ - a relatively minor change.

The simulations were set to run for a maximum of 100 million years, but were brought to a premature end if one or other of the planets were ejected from the system or collided with the central body. Simulations were also curtailed if the two planets collided with one another. For each of these conditions, the time at which the simulation finished was recorded, allowing us to create dynamical maps of the system to examine the dynamical context of the orbits presented above, and to see whether the system was dynamically feasible. Such maps have, in the past, revealed certain systems to be dynamically unfeasible (e.g. Horner et al. 2011; Wittenmyer et al. 2012b; Horner et al. 2013, 2014). In other cases, dynamical mappings have resulted in stronger constraints for a given system's orbits than was possible solely on the grounds of the observational data (e.g. Wittenmyer et al. 2012c; Robertson et al. 2012; Wittenmyer et al. 2014c). Dynamical simulations therefore offer the potential to help distinguish between different solutions with similar goodness of fit, such as those proposed in this work, as well as yielding an important dynamical 'sanity check'.

To complement these dynamical simulations, we also chose to trial a new technique for the dynamical analysis of newly discovered systems. Rather than populate regular grids in

element space, whilst holding the better constrained planet's initial orbit fixed, we instead performed repeated fits to the observational data. In our fitting, we required solely that the solutions produced lie within $3\sigma$ of the best-fit solution, allowing all parameters to vary freely. This created clouds of 'potential solutions' distributed around the best fit out to a range of $\chi^2_{best} + 9$. We then randomly selected solutions to evenly sample the phase space between the best-fit solution (at $\chi^2_{best}$) and $\chi^2_{best} + 9$. As before, we generated 126,075 unique solutions for each of the two scenarios presented above.

Where our traditional dynamical maps explore the dynamical context of the solutions in a readily apparent fashion, these new simulations are designed to instead examine the stability of the system as a function of the goodness of fit of the orbital solution. In addition, they allow us to explore the stability as a function of the masses assigned to the two planets in question. As such, they provide a natural complement to the traditional maps, as can be seen below.

## 5. Dynamical Stability Results

Figure 6 shows the dynamical context of the short period solution for the two planet HD 30177 system, as described in Table 4. The best fit solution lies in an area of strong dynamical instability, with the majority of locations within the $1\sigma$ uncertainty range being similarly unstable. There is, however, a small subset of solutions in that range that are stable, marking the inner edge of a broad stable region seen towards larger semi-major axes and smaller eccentricities. The small island of stability at $a \sim 5.687$ au is the result of the planets becoming trapped in mutual 2:1 mean-motion resonance, whilst the narrow curved region of moderate stability at high eccentricities is caused by orbits for HD 30177c with periastron located at the semi-major axis of HD 30177b. Dynamical stability for the system on near-circular, non-resonant orbits is only seen in these simulations exterior to the planet's mutual 3:1 mean-motion resonance, located at $a \sim 7.453$ au (and the cause of the small island of stability at non-zero eccentricities at that semi-major axis). As a result, these simulations suggest that the short-period solution is not dynamically favoured, unless the orbital period for HD 30177c is significantly longer than the best fit, the orbit markedly less eccentric, or if the two planets are trapped in mutual 3:1 mean motion resonance.

These results are strongly supported by our subsidiary integrations - the results of which are shown in Figures 7-8. Figure 7 shows the stability of the candidate HD 30177 planetary systems as a function of the eccentricities of the two planets, their period ratio, and the goodness of the fit of the solution tested. In Figure 7, the upper plots show all solutions within $3\sigma$ of the best fit, whilst the lower show only those solutions within $1\sigma$ of the best fit.

It is immediately apparent that truly stable solutions are limited to only a very narrow range of the plots - namely two narrow regions with low eccentricities, and widely separated orbits. In fact, these solutions all lie at, or somewhat outside, the location of the 3:1 mean motion resonance between the two planets (P1/P2 $\sim$ 0.33). The inner of the two stable patches are those orbits that are resonant, whilst the outermost are those sufficiently separated to be exterior to that resonance. Even at these stable separations, the system is only feasible for low-to-moderate planetary eccentricities - solutions that ascribe an eccentricity of $\sim$ 0.25 or greater to either planet prove strongly unstable.

Figure 8 shows the influence of the mass of the two planets on the stability of the solution. The resonant and extra-resonant stable regions are again clearly visible, and it is apparent that the masses of the two planets seem to have little influence on the stability of the solution. A slight influence from the planetary mass can be seen in the middle row of Figure 8, which shows that stable solutions with the lowest cumulative planet mass (i.e. $M_b + M_c$) have slightly higher mean eccentricities than those for larger cumulative masses. This effect is only weak, and is the result of the least massive solutions veering away from lower eccentricities. Given that the eccentricities of planetary orbits tend to be somewhat over-estimated when fitting radial velocity data (O'Toole et al. 2009), this may be an indication that the lower-mass solutions are slightly less favourable than their higher mass counterparts.

Finally, the bottom row of Figure 8 shows the stability of the solution clouds as a function of the maximum eccentricity between the two planets (i.e. the value plotted on the y-axis is whichever is greater of $e_b$ and $e_c$). This reinforces the result from Figure 7 that solutions with either of the two planets moving on orbits with $e \geq 0.25$ are unstable regardless of their separation, or the mass of the planets involved.

Taken in concert, our results show that, whilst short-period solutions for the HD 30177 system can prove dynamically stable, they require the two planets to either be trapped in mutual 3:1 mean motion resonance, or to be more widely spaced, and further require that neither planet move on an orbit with eccentricity greater than 0.25.

But what of our alternative, longer-period solution for the planetary system? Figure 9 shows the dynamical context of that solution. Unlike the short period solution, the two planets are now sufficiently widely separated that the great majority of orbits around the best-fit solution are now dynamically stable for the full 100 Myr of our simulations. At the very inner edge of the plot, the cliff of instability exterior to the planet's mutual 3:1 mean-motion resonance can again be seen, as can hints of the moderate stability afforded by the periastron of HD 30177 c falling at the semi-major axis of HD 30177 b (top left of the plot). Purely on the basis of this plot, the longer-period solution seems markedly more

dynamically feasible, a result once again borne out by the plots of our subsidiary simulations of the long-period solution (Figures 10-13).

Figure 10 reveals many of the same features as Figure 9 - a significant proportion of the solutions are dynamically stable - particularly those within $1\sigma$ of the best fit (lower panels). The greater the orbital separation of the two planets, the greater can be their orbital eccentricities before destabilising the system. In addition, however, the destabilising influence of distant mean-motion resonances is revealed in these plots, as the notches of instability carved into the distribution at specific period ratios. Aside from these few unstable regions, however, the great majority of solutions within $1\sigma$ of the best fit are stable.

Figure 11 shows that the mass ratio of the planets (left hand plots) has little or no influence on their stability. Interestingly, though, the lower-right hand panel reveals an apparent relationship in the fitting between the cumulative mass of the planets and their mutual separation. The more widely separated the two planets (and hence the more distant is HD 30177c), the greater their cumulative mass. This is not at all surprising: the more distant HD 30177c is, the greater its mass would have to be to achieve a radial velocity signal of a given amplitude. This feature is therefore entirely expected, but nevertheless serves to nicely illustrate the relationship between different parameters in the radial velocity fitting process.

Figure 12 again reveals that the more eccentric the orbits of the planets, the more likely they are to prove unstable - although once again, the great majority of the sampled phase-space proves dynamically stable. More interesting, however, are the results shown in Figure 13. The left-hand panels of that plot, which show the stability of the solutions as a function of the maximum eccentricity between the two panels (y-axis) and the mass ratio of the two planets (x-axis) suggest that, the closer the two planetary masses are to parity, the more likely eccentric orbits are to be stable. By contrast, the lower-right hand plot suggests that the greater the sum of the planetary masses, the more likely solutions with high eccentricities are to be stable. Taken in concert, these results are once again a reflection of the relationship between cumulative mass and orbital separation. That is, the greater the orbital separation of the two planets, the greater their cumulative mass, and the closer to parity their masses become (since our fits suggest that HD 30177c is the less massive of the two). At the same time, we saw from Figure 10 that, the greater the separation of the two planets, the more stable are those orbital solutions at higher eccentricity. So once again, we are looking at the same thing - these two apparent trends are the result of the requirement that a more distant HD 30177c must be more massive in order to generate the observed radial velocity amplitude.

## 6.   Conclusions

We present the results of new radial velocity observations of HD 30177, which reveal for the first time the presence of a second, long-period planet in that system. Two possible orbital solutions for the planetary system are presented - one with a shorter-period orbit for HD 30177 c, and one with the two planets more widely spaced, and HD 30177 c on a longer period orbit. The two solutions are virtually indistinguishable from one another in terms of the quality of fit that they provide to the data. However, the short-period solution placed the two planets on orbits sufficiently compact that they lie closer than their mutual 3:1 mean-motion resonance.

Although several highly compact multi-planet systems have been discovered in recent years, it has become apparent that such compact systems rely on dynamical stability conferred by mutual resonant planetary orbits. As such, it seemed prudent to build on our earlier work, and carry out detailed $n$-body simulations of the two potential solutions for the HD 30177 system, to see whether it was possible to rule either out on dynamical stability grounds.

Our results reveal that, although some stable solutions can be found for the short-period variant of the HD 30177 system, those solutions require orbital eccentricities for the planets that are typically smaller than given by the best fit solution, and require HD 30177 c to be somewhat more distant than the best fit. In other words, the require relatively low eccentricity orbits for that planet exterior to its mutual 3:1 mean-motion resonance with HD 30177 b. By contrast, the great majority of the longer-period solutions tested proved dynamically stable - and across a much greater range of potential semi-major axes and orbital eccentricities.

As a result, we consider that the most likely solution for the orbit of HD 30177c is the longer period option: an m sin $i$ = 7.6±3.1 $M_{\rm Jup}$ planet with $a$ = 9.89 ± 1.04 au, $e$ = 0.22 ± 0.14, and an orbital period of $P$ = 11613 ± 1837 days. We note that for inclinations $i \lesssim 30^{\rm o}$, the two orbiting bodies in the HD 30177 system fall into the brown dwarf regime. With an orbital separation of $a \sim 10$ au, one can consider HD 30177c to be one of the first members of an emerging class of "Saturn analogs," referring to planets with orbital separations similar to Saturn. Just as long-term radial velocity surveys have begun to characterize "Jupiter analogs" (Wittenmyer et al. 2011; Rowan et al. 2016; Wittenmyer et al. 2016b), the continuation of legacy surveys such as the Anglo-Australian Planet Search will enable us to probe the population of planets in Saturn-like orbits in the coming decade.

## REFERENCES

Adibekyan, V. Z., Sousa, S. G., Santos, N. C., et al. 2012, A&A, 545, A32

Anglada-Escudé, G., & Butler, R. P. 2012, ApJS, 200, 15

Borucki, W. J., Koch, D. G., Basri, G., et al. 2011, ApJ, 736, 19

Butler, R. P., Marcy, G. W., Williams, E., McCarthy, C., Dosanjh, P., & Vogt, S. S. 1996, PASP, 108, 500

Butler, R. P., Wright, J. T., Marcy, G. W., et al. 2006, ApJ, 646, 505

Chambers, J. E. 1999, MNRAS, 304, 793

Coughlin, J. L., Mullally, F., Thompson, S. E., et al. 2016, ApJS, 224, 12

Dumusque, X., Lovis, C., Ségransan, D., et al. 2011, A&A, 535, A55

Endl, M., Brugamyer, E. J., Cochran, W. D., et al. 2016, ApJ, 818, 34

Fang, J., & Margot, J.-L. 2012, ApJ, 761, 92

Feng, Y. K., Wright, J. T., Nelson, B., et al. 2015, ApJ, 800, 22

Fischer, D., Anglada-Escude, G., Arriagada, P., et al. 2016, arXiv:1602.07939

Franchini, M., Morossi, C., Marcantonio, P. D., Malagnini, M. L., & Chavez, M. 2014, MNRAS, 442, 220

Ghezzi, L., Cunha, K., Smith, V. V., et al. 2010, ApJ, 720, 1290

Han, E., Wang, S. X., Wright, J. T., et al. 2014, PASP, 126, 827

Hébrard, É. M., Donati, J.-F., Delfosse, X., et al. 2014, MNRAS, 443, 2599

Hinse, T. C., Horner, J., & Wittenmyer, R. A. 2014, Journal of Astronomy and Space Sciences, 31, 187

Horner, J., & Jones, B. W. 2008, International Journal of Astrobiology, 7, 251

Horner, J., & Jones, B. W. 2010b, International Journal of Astrobiology, 9, 273

Horner, J., Jones, B. W., & Chambers, J. 2010, International Journal of Astrobiology, 9, 1

Horner, J., Marshall, J. P., Wittenmyer, R. A., & Tinney, C. G. 2011, MNRAS, 416, L11

Horner, J., Wittenmyer, R. A., Hinse, T. C., et al. 2013, MNRAS, 435, 2033

Horner, J., Wittenmyer, R. A., Hinse, T. C., & Marshall, J. P. 2014, MNRAS, 439, 1176

Houk, N., & Cowley, A. P. 1975, University of Michigan Catalogue of two-dimensional spectral types for the HD stars. Volume I. Declinations -90‿ to -53°., by Houk, N.; Cowley, A. P.. Ann Arbor, MI (USA): Department of Astronomy, University of Michigan, 19 + 452 p.,

Howard, A. W., Johnson, J. A., Marcy, G. W., et al. 2010, ApJ, 721, 1467

Jones, H. R. A., Butler, R. P., Tinney, C. G., et al. 2010, MNRAS, 403, 1703

Kennedy, G. M., Wyatt, M. C., Bryden, G., Wittenmyer, R., & Sibthorpe, B. 2013, MNRAS, 436, 898

Lewis, A. R., Quinn, T., & Kaib, N. A. 2013, AJ, 146, 16

Lovis, C., Dumusque, X., Santos, N. C., et al. 2011, arXiv:1107.5325

Marmier, M., Ségransan, D., Udry, S., et al. 2013, A&A, 551, A90

Marshall, J., Horner, J., & Carter, A. 2010, International Journal of Astrobiology, 9, 259

Meschiari, S., Wolf, A. S., Rivera, E., et al. 2009, PASP, 121, 1016

Moutou, C., Lo Curto, G., Mayor, M., et al. 2015, A&A, 576, A48

O'Toole, S. J., Tinney, C. G., Jones, H. R. A., et al. 2009, MNRAS, 392, 641

Robertson, P., Horner, J., Wittenmyer, R. A., et al. 2012, ApJ, 754, 50

Robertson, P., Endl, M., Cochran, W. D., et al. 2012, ApJ, 749, 39

Rowan, D., Meschiari, S., Laughlin, G., et al. 2016, ApJ, 817, 104

Rowe, J. F., Bryson, S. T., Marcy, G. W., et al. 2014, ApJ, 784, 45

Santos, N. C., Sousa, S. G., Mortier, A., et al. 2013, A&A, 556, A150

Sousa, S. G., Santos, N. C., Israelian, G., Mayor, M., & Udry, S. 2011, A&A, 533, A141

Takeda, G., Ford, E. B., Sills, A., et al. 2007, ApJS, 168, 297

Tinney, C. G., Butler, R. P., Marcy, G. W., et al. 2001, ApJ, 551, 507

Tinney, C. G., Butler, R. P., Marcy, G. W., et al. 2003, ApJ, 587, 423

Tinney, C. G., Wittenmyer, R. A., Butler, R. P., et al. 2011, ApJ, 732, 31

Valenti, J. A., Butler, R. P. & Marcy, G. W. 1995, PASP, 107, 966.

van Leeuwen, F. 2007, A&A, 474, 653

Wittenmyer, R. A., Tinney, C. G., O'Toole, S. J., et al. 2011, ApJ, 727, 102

Wittenmyer, R. A., Horner, J., Tuomi, M., et al. 2012a, ApJ, 753, 169

Wittenmyer, R. A., Horner, J., Marshall, J. P., Butters, O. W., & Tinney, C. G. 2012b, MNRAS, 419, 3258

Wittenmyer, R. A., Horner, J., & Tinney, C. G. 2012, ApJ, 761, 165

Wittenmyer, R. A., Wang, S., Horner, J., et al. 2013, ApJS, 208, 2

Wittenmyer, R. A., Horner, J., Tinney, C. G., et al. 2014a, ApJ, 783, 103

Wittenmyer, R. A., Tuomi, M., Butler, R. P., et al. 2014b, ApJ, 791, 114

Wittenmyer, R. A., Tan, X., Lee, M. H., et al. 2014c, ApJ, 780, 140

Wittenmyer, R. A., Butler, R. P., Wang, L., et al. 2016a, MNRAS, 455, 1398

Wittenmyer, R. A., Butler, R. P., Tinney, C. G., et al. 2016b, ApJ, 819, 28

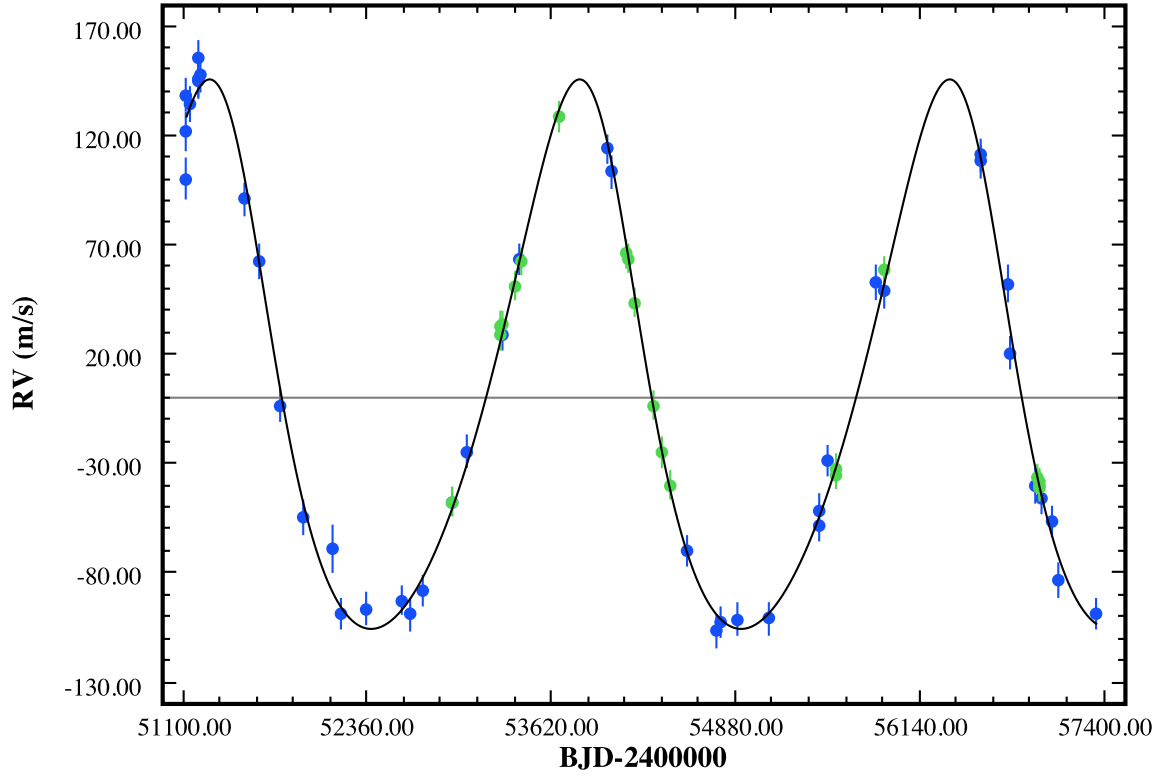Wright, J. T., Fakhouri, O., Marcy, G. W., et al. 2011, PASP, 123, 412

Fig. 1.— Data and Keplerian model fit for the inner planet HD 30177b. AAT – blue; HARPS – green. The orbit of the outer planet has been removed. We have added $6\,\mathrm{m\,s^{-1}}$ of jitter in quadrature to the uncertainties, and this fit has an rms of $7.07\,\mathrm{m\,s^{-1}}$.
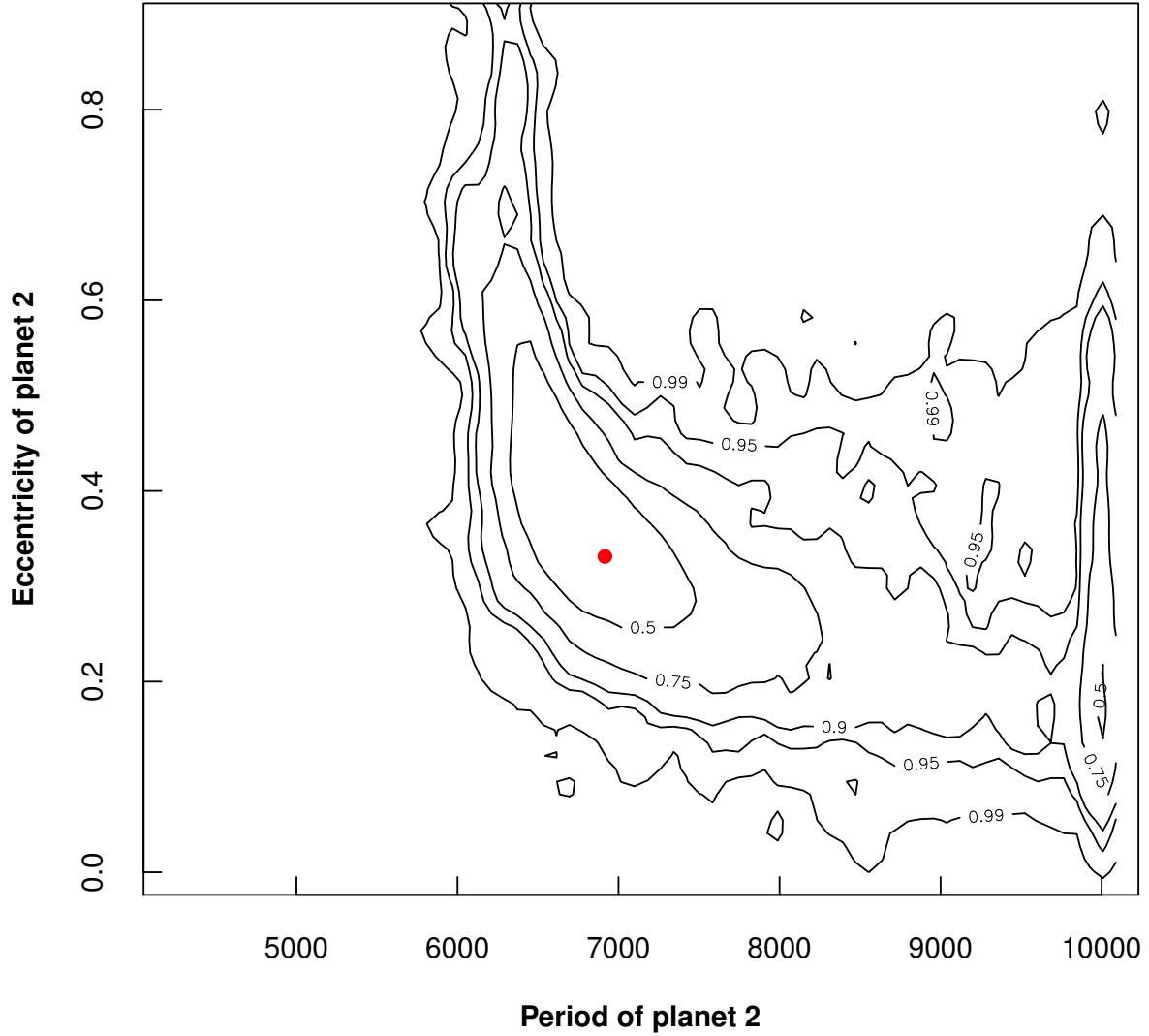
Fig. 2.— Contours of $\chi^2$ as a function of the outer planet's eccentricity and orbital period. Contours are labeled with confidence intervals around the best fit (red dot). Hints of a second local $\chi^2$ minimum can be seen in the lower right, at long periods and low eccentricities.

Table 1.   Stellar Parameters for HD 30177

| Parameter | Value | Reference |
|---|---|---|
| Spec. Type | G8 V | Houk & Cowley (1975) |
| Distance (pc) | 54.7±2.3 | van Leeuwen (2007) |
| Mass ($M_\odot$) | $0.951^{+0.093}_{-0.053}$ | Takeda et al. (2007) |
| | 1.05±0.08 | Santos et al. (2013) |
| | 0.988±0.033 | Sousa et al. (2011) |
| V sin $i$ (km  s$^{-1}$) | 2.96±0.50 | Butler et al. (2006) |
| [$Fe/H$] | +0.33±0.05 | Franchini et al. (2014) |
| | 0.37±0.06 | Adibekyan et al. (2012) |
| | 0.39±0.05 | Ghezzi et al. (2010) |
| | 0.394±0.030 | Butler et al. (2006) |
| $T_{eff}$ (K) | 5580±12 | Franchini et al. (2014) |
| | 5601±73 | Adibekyan et al. (2012) |
| | 5595±50 | Ghezzi et al. (2010) |
| | 5607±44 | Butler et al. (2006) |
| log $g$ | 4.41±0.12 | Franchini et al. (2014) |
| | 4.34±0.05 | Sousa et al. (2011) |
| | 4.15±0.13 | Ghezzi et al. (2010) |
| | 4.31±0.06 | Butler et al. (2006) |
| Age (Gyr) | $11.6^{+1.8}_{-2.2}$ | Takeda et al. (2007) |
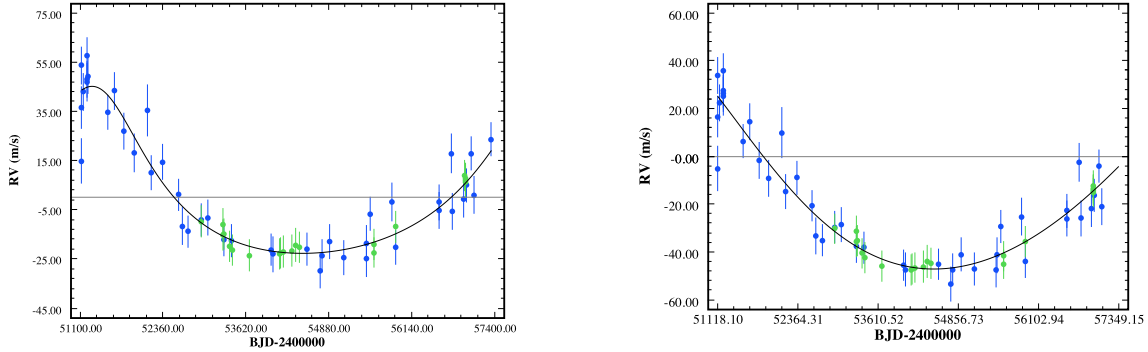


Fig. 3.— Data and Keplerian model fit for the outer planet HD 30177c. AAT – blue; HARPS – green. The orbit of the inner planet has been removed. We have added $6\,\mathrm{m\,s^{-1}}$ of jitter in quadrature to the uncertainties. Left panel: Nominal best fit, with $P = 6921$ d. Right panel: Long-period solution, with $P = 11640$ d.

Table 2.   AAT Radial Velocities for HD 30177

| BJD-2400000 | Velocity ($\mathrm{m\,s^{-1}}$) | Uncertainty ($\mathrm{m\,s^{-1}}$) |
|---|---|---|
| 51118.09737 | 227.2 | 4.5 |
| 51119.19240 | 188.6 | 6.9 |
| 51121.15141 | 210.7 | 6.1 |
| 51157.10219 | 223.5 | 4.5 |
| 51211.98344 | 234.6 | 5.0 |
| 51212.96597 | 235.8 | 4.2 |
| 51213.99955 | 245.4 | 4.0 |
| 51214.95065 | 237.3 | 3.6 |
| 51525.99718 | 177.1 | 3.4 |
| 51630.91556 | 144.9 | 4.6 |
| 51768.32960 | 73.4 | 4.2 |
| 51921.10749 | 14.8 | 4.6 |
| 52127.32049 | -9.2 | 8.5 |
| 52188.25324 | -41.3 | 3.6 |
| 52358.91806 | -45.6 | 3.8 |
| 52598.18750 | -49.8 | 2.0 |
| 52655.02431 | -57.6 | 4.4 |
| 52747.84861 | -49.0 | 2.2 |
| 52945.18132 | -12.7 | 2.6 |
| 53044.03464 | 8.2 | 3.6 |
| 53282.26188 | 58.2 | 2.8 |
| 53400.99440 | 91.4 | 2.5 |
| 54010.25007 | 137.4 | 1.8 |
| 54038.21420 | 126.4 | 3.4 |
| 54549.93698 | -47.3 | 2.2 |
| 54751.25707 | -83.8 | 3.8 |
| 54776.17955 | -79.6 | 2.2 |
| 54900.95132 | -78.0 | 3.4 |
| 55109.18072 | -77.0 | 3.2 |
| 55457.26529 | -32.2 | 3.9 |
| 55461.28586 | -25.3 | 4.3 |
| 55519.17942 | -2.1 | 3.3 |
| 55845.21616 | 82.2 | 4.7 |
| 55899.10987 | 79.0 | 3.2 |
| 56555.28257 | 149.0 | 4.1 |
| 56556.25219 | 152.0 | 3.6 |
| 56746.90702 | 97.7 | 5.1 |
| 56766.86295 | 66.2 | 4.0 |
| 56935.25257 | 10.2 | 4.0 |
| 56970.23271 | 5.6 | 3.0 |
| 57052.02821 | -2.2 | 3.0 |
| 57094.90039 | -28.0 | 4.6 |
| 57349.14648 | -34.5 | 3.1 |

Table 3.   HARPS-TERRA Radial Velocities for HD 30177

| BJD-2400000 | Velocity ($\mathrm{m\,s^{-1}}$) | Uncertainty ($\mathrm{m\,s^{-1}}$) |
|---|---|---|
| 52947.76453 | -70.7 | 1.6 |
| 53273.88347 | 0.0 | 1.9 |
| 53274.88548 | 4.6 | 1.9 |
| 53288.84830 | 4.6 | 1.5 |
| 53367.68146 | 21.6 | 1.8 |
| 53410.60057 | 32.3 | 1.5 |
| 53669.80849 | 95.9 | 2.0 |
| 54137.58873 | 31.0 | 1.5 |
| 54143.51190 | 28.9 | 1.4 |
| 54194.47989 | 8.6 | 1.5 |
| 54315.91894 | -38.8 | 2.3 |
| 54384.87123 | -60.3 | 3.2 |
| 54431.68520 | -75.4 | 1.9 |
| 55563.54385 | -63.1 | 1.0 |
| 55564.57743 | -66.2 | 0.8 |
| 55903.70118 | 30.9 | 2.2 |
| 56953.81794 | -43.4 | 0.7 |
| 56955.78182 | -45.2 | 0.7 |
| 56957.88054 | -46.5 | 1.1 |
| 56959.68147 | -47.8 | 0.8 |

Table 4.   HD 30177 Planetary System Parameters (all data)

| Parameter | Nominal Best Fit | | Long-Period Solution | |
|---|---|---|---|---|
| | HD 30177b | HD 30177c | HD 30177b | HD 30177c |
| Period (days) | 2532.5±10.6 | 6921±621 | 2520.6±8.9 | 11640±2432 |
| Eccentricity | 0.189±0.014 | 0.35±0.10 | 0.188±0.014 | 0.14±0.11 |
| $\omega$ (degrees) | 32±4 | 11±13 | 30±4 | 32±48 |
| $K$ ($\mathrm{m\,s^{-1}}$) | 126.1±1.9 | 35.8±3.4 | 126.9±1.7 | 59.4±27.6 |
| $T_0$ (BJD-2400000) | 51428±26 | 51661±573 | 51434±24 | 48426±2978 |
| m sin $i$ ($\mathrm{M_{Jup}}$) | 8.07±0.12 | 3.0±0.3 | 8.11±0.11 | 6.4±3.3 |
| $a$ (au) | 3.58±0.01 | 6.99±0.42 | 3.57±0.01 | 9.9±1.4 |
| RMS of fit ($\mathrm{m\,s^{-1}}$) | 7.04 | | 7.17 | |
| $\chi_\nu^2$ (51 d.o.f.) | 0.98 | | 1.01 | |
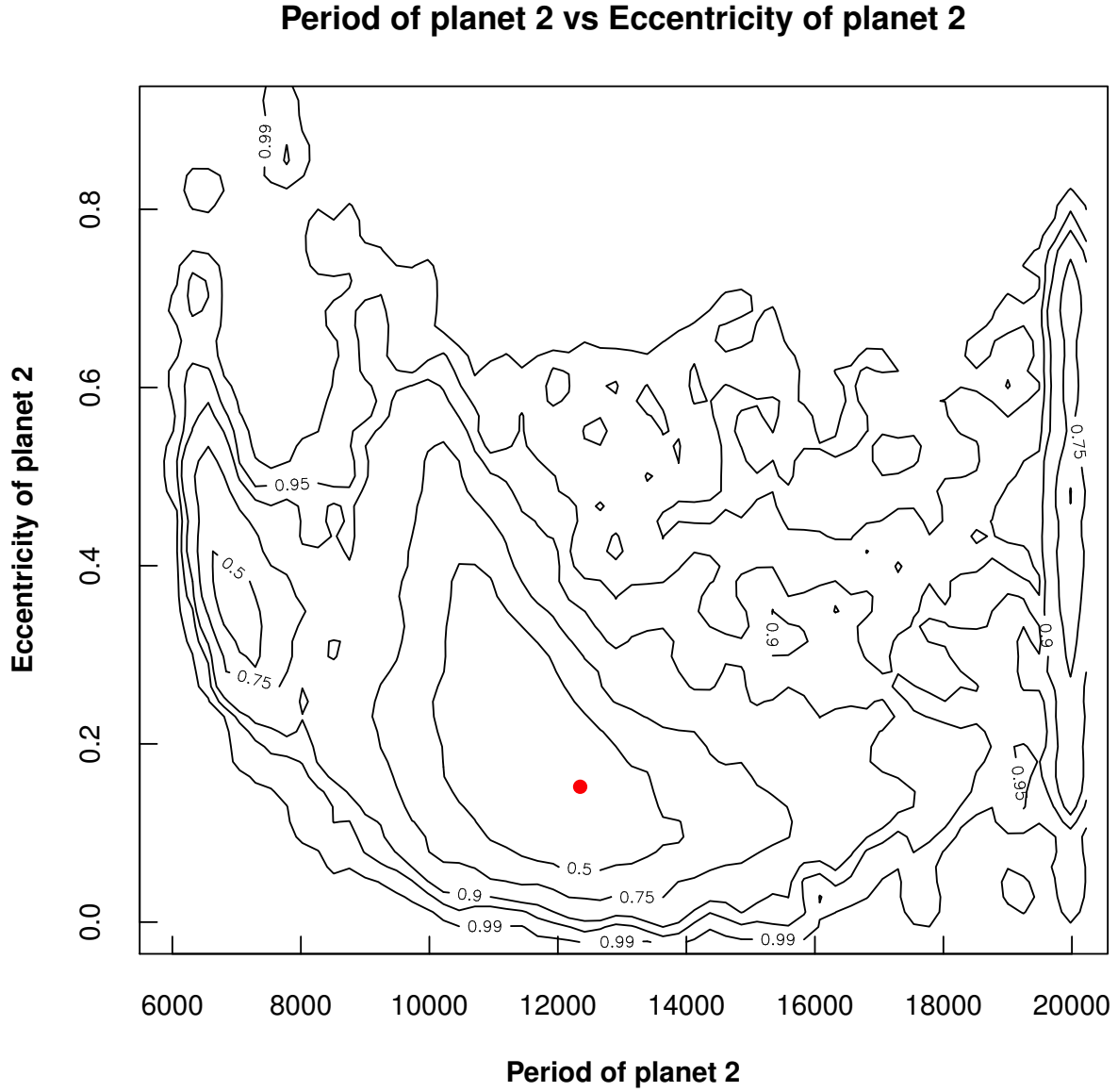
Fig. 4.— Same as Figure 2, but for the long-period solution where one outlier data point has been removed. Two local $\chi^2$ minima are evident, with the longer-period solution at lower eccentricity (red dot).
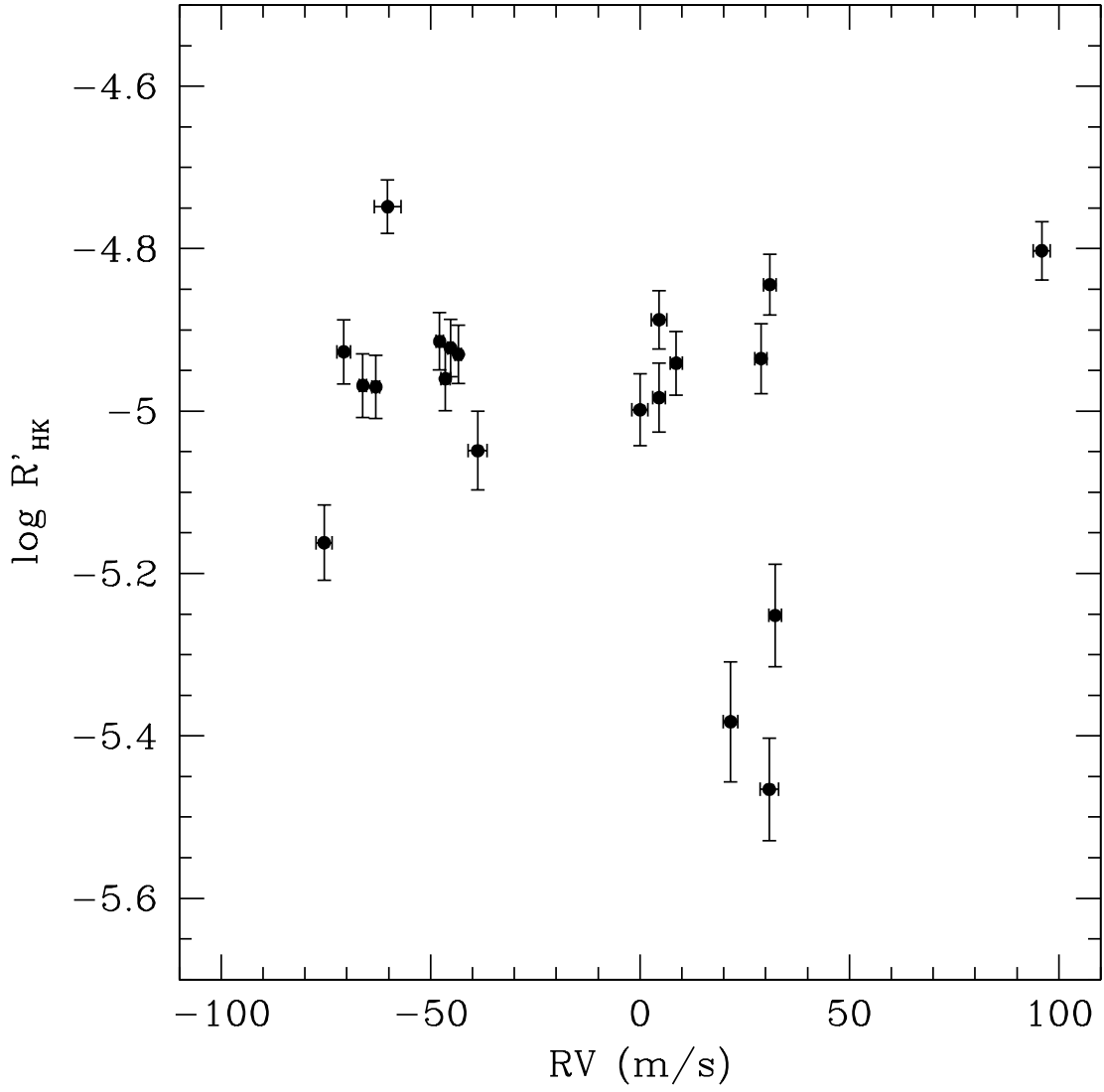
Fig. 5.— Ca II activity index $\log R'_{HK}$ as a function of radial velocity for the HARPS spectra of HD 30177. No correlation is evident from the 11 years of data, and hence we conclude that a stellar magnetic cycle is not responsible for the observed radial velocity variations.

Table 5.    HD 30177 Planetary System Parameters (outlier removed)

| Parameter | Nominal Best Fit | | Long-Period Solution | |
|---|---|---|---|---|
| | HD 30177b | HD 30177c | HD 30177b | HD 30177c |
| Period (days) | 2531.3±11.3 | 7601±1134 | 2524.4±9.8 | 11613±1837 |
| Eccentricity | 0.185±0.012 | 0.31±0.11 | 0.184±0.012 | 0.22±0.14 |
| $\omega$ (degrees) | 32±4 | 13±16 | 31±3 | 19±30 |
| $K$ (m s$^{-1}$) | 125.8±1.7 | 37.9±3.8 | 126.3±1.5 | 70.8±29.5 |
| $T_0$ (BJD-2400000) | 51430±27 | 52154±2009 | 51434±29 | 48973±1211 |
| m sin $i$ (M$_{\rm Jup}$) | 8.06±0.11 | 3.32±0.45 | 8.08±0.10 | 7.6±3.1 |
| $a$ (au) | 3.58±0.01 | 7.45±0.75 | 3.58±0.01 | 9.89±1.04 |
| RMS of fit (m s$^{-1}$) | 5.98 | | 6.01 | |
| $\chi_\nu^2$ (50 d.o.f.) | 0.76 | | 0.77 | |
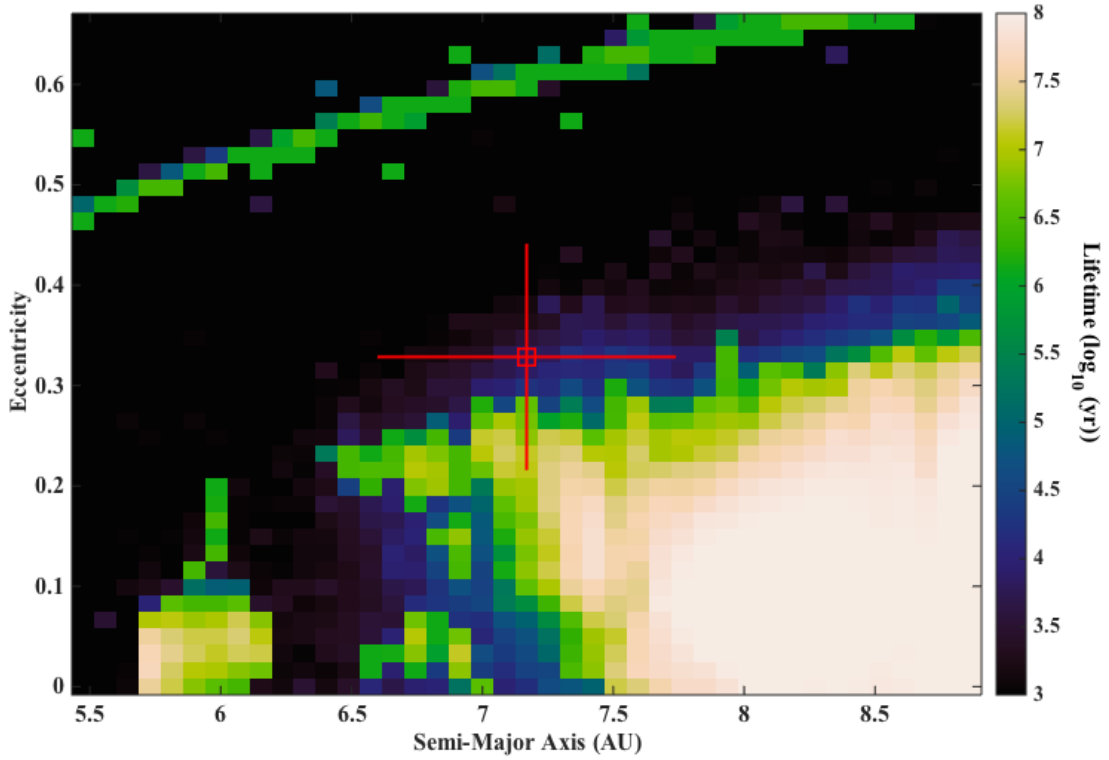


Fig. 6.— The dynamical stability of the short-period solution for the orbit of HD 30177c, as a function of semi-major axis and eccentricity. The red box, to the centre of the plot, denotes the location of the best-fit solution, whilst the lines radiating from that point show the $1 - \sigma$ uncertainties. It is immediately apparent that the best-fit solution lies in a region of significant dynamical instability.
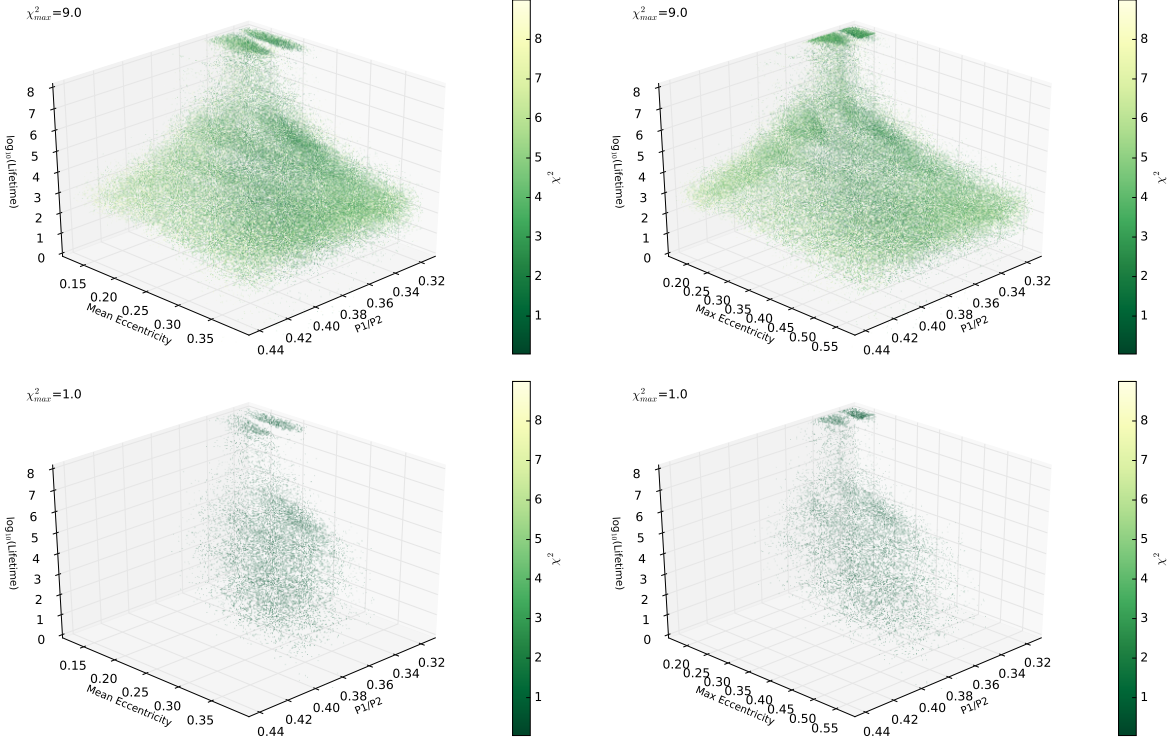
Fig. 7.— The stability of the short-period solution for HD30177, as a function of the mean (left) and maximum (right) eccentricity of the two planets in the system. The colour axis shows the goodness of fit for each of the solutions tested, with the vertical axis showing the lifetime, and the y-axis the ratio of the two planetary orbital periods. The upper plots show the results for solutions within 3 $\sigma$ of the best fit, whilst the lower show only those simulations within 1 $\sigma$ of that solution. We note that animated versions of the figures are available in the online edition of this work, which may help the reader to fully visualise the relationship between the stability and the various variables considered.
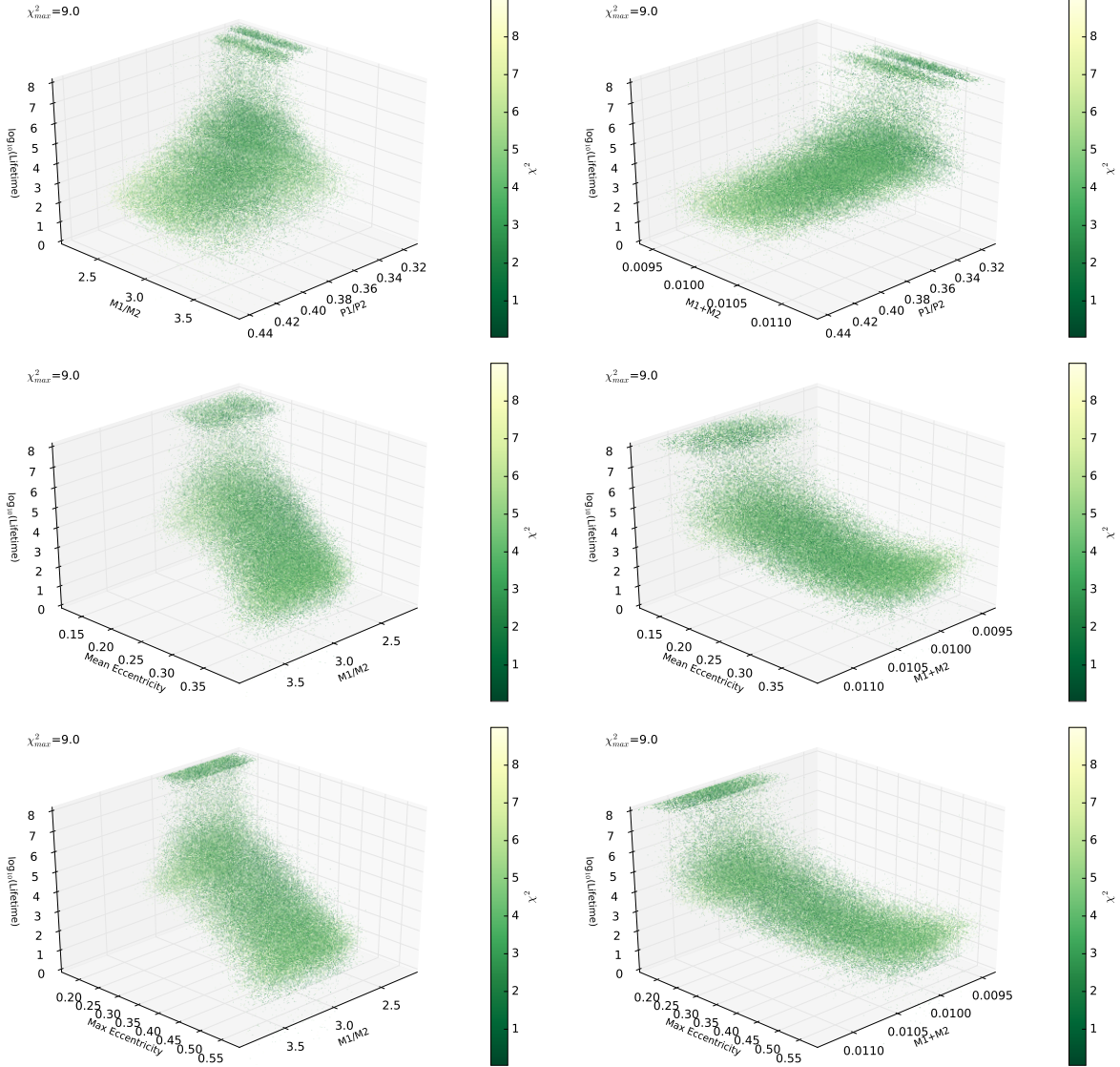
Fig. 8.— *Upper row:* The stability of the short-period solution for HD 30177c, as a function of the mass ratio (left) and total mass (right) of the two planets in the system. The color scale shows the goodness of fit for each of the solutions tested, with the vertical axis showing the lifetime, and the y-axis the ratio of the two planetary orbital periods. Results for solutions within 3 $\sigma$ of the best fit are shown. *Middle row:* Same, but the x-axis now denotes the mean eccentricity of the planetary orbits. *Bottom row:* Same, but the x-axis now denotes the maximum eccentricity of the planetary orbits. Animated versions of the figures are provided in the online version of the paper.
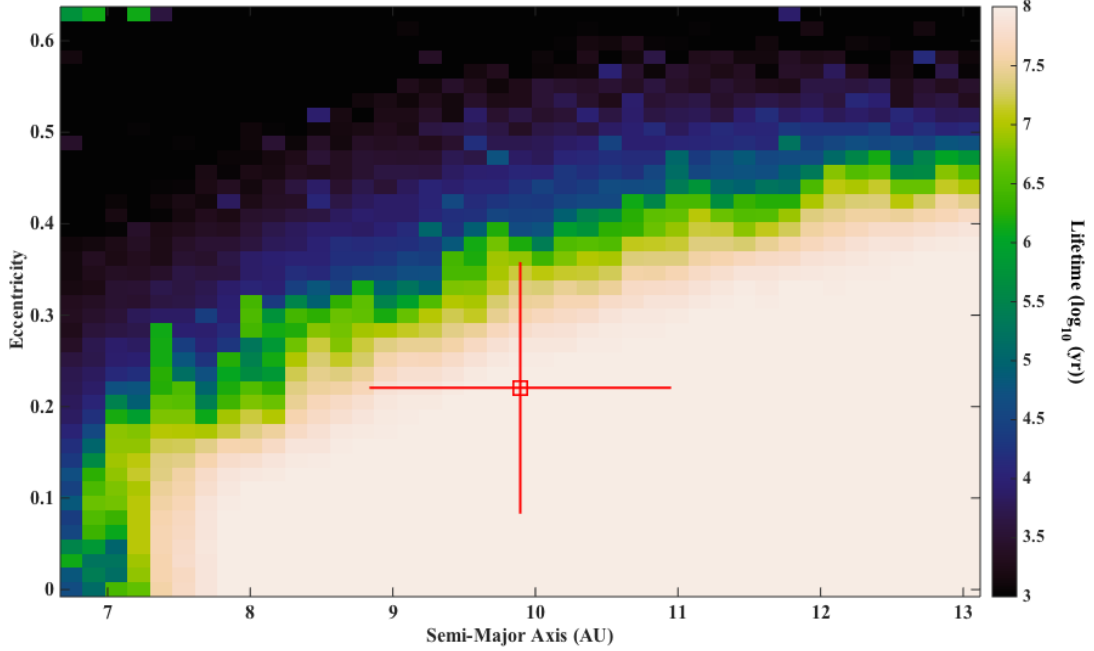
Fig. 9.— The stability of the long-period solution for the orbit of HD 30177c, as a function of semi-major axis and eccentricity. As with Figure 6, the red box marks the location of the best-fit solution, with the red lines radiating showing the $1 - \sigma$ uncertainties. Unlike the short-period solution, the best-fit orbit now lies in a broad region of dynamical stability, with most solutions within $1 - \sigma$ proving stable for the full 100 Myr of our integrations.
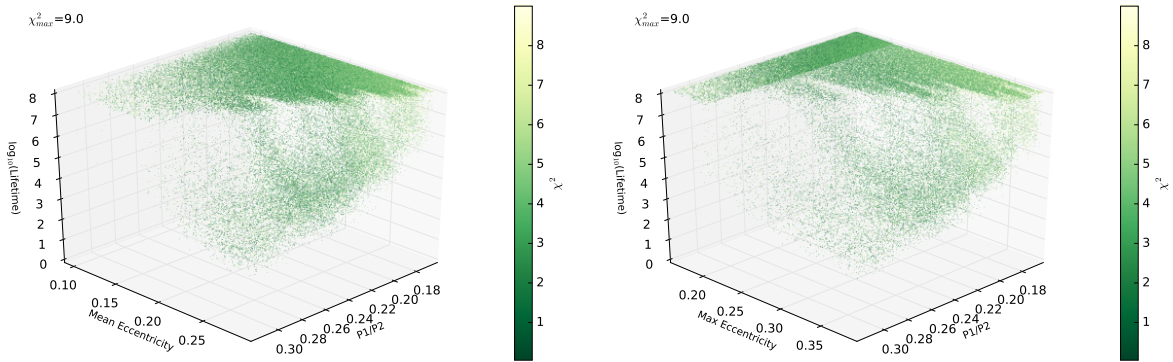


Fig. 10.— The stability of the long-period solution for HD 30177, as a function of the mean (left) and maximum (right) eccentricity of the two planets in the system. The color scale and axes have the same meaning as in Figure 7. The upper plots show the results for solutions within $3\ \sigma$ of the best fit, whilst the lower show only those simulations within $1\ \sigma$ of that solution. Animated versions of the figures are provided in the online version of the paper.
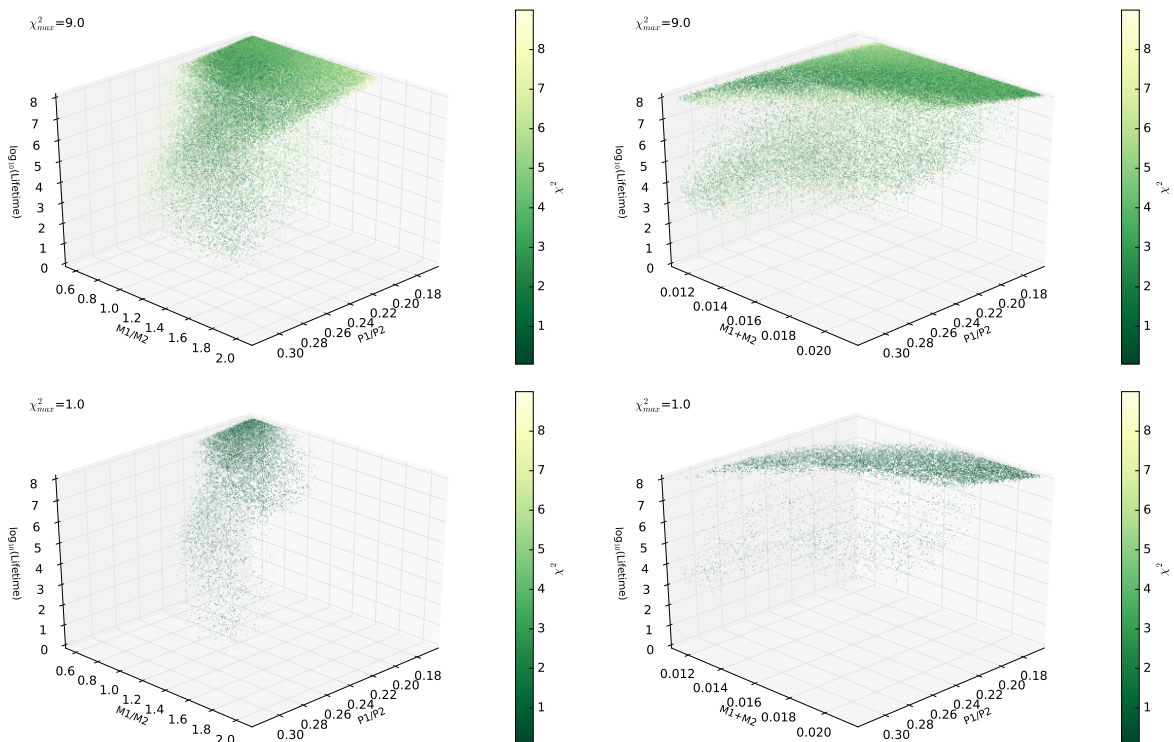
Fig. 11.— The stability of the long-period solution for HD 30177, as a function of the mass ratio (left) and total mass (right) of the two planets in the system. As before, the colour axis shows the goodness of fit for each of the solutions tested, with the vertical axis showing the lifetime, and the y-axis the ratio of the two planetary orbital periods. Solutions within $3\,\sigma$ of the best fit are shown in the upper panels, and only those within $1\sigma$ are shown in the lower panels. Animated versions of the figures are provided in the online version of the paper.
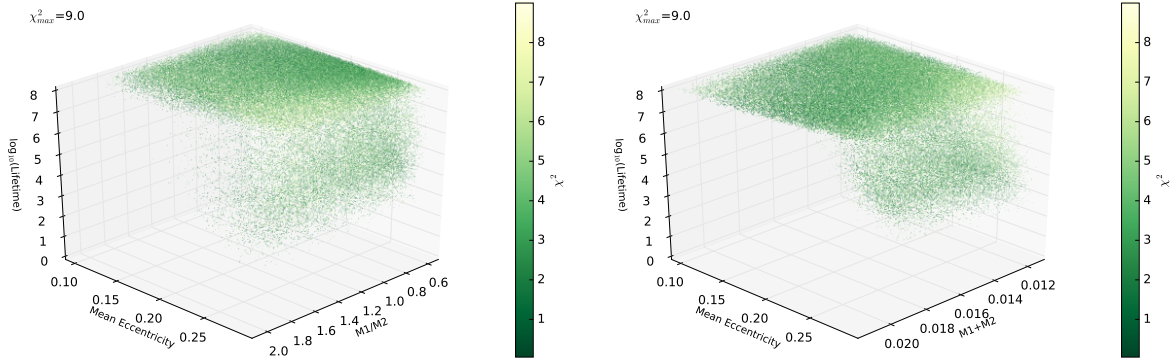
Fig. 12.— The stability of the long-period solution for HD 30177, again as a function of the mass ratio (left) and total mass (right) of the two planets in the system. Again, the colour axis shows the goodness of fit for each of the solutions tested, with the vertical axis showing the lifetime, and the x-axis the mean eccentricity of the planetary orbits. Results for solutions within 3 $\sigma$ of the best fit are shown. Animated versions of the figures are provided in the online version of the paper.
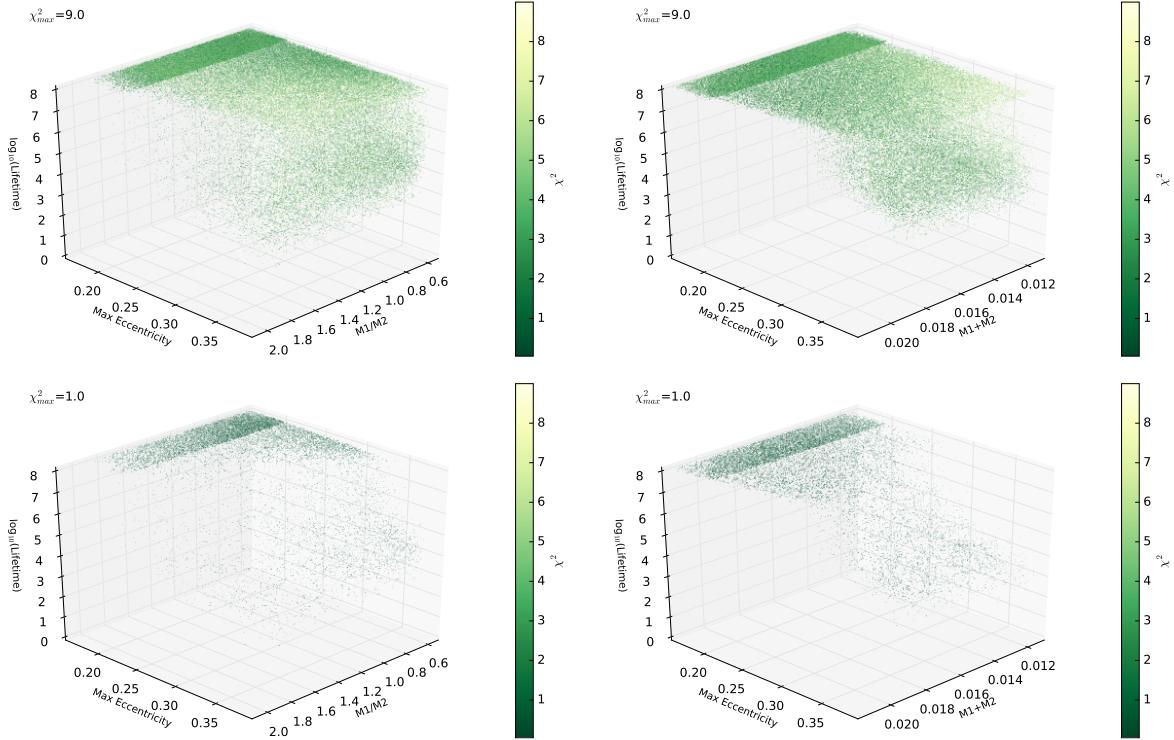
Fig. 13.— The stability of the long-period solution for HD 30177, again as a function of the mass ratio (left) and total mass (right) of the two planets in the system. The colour axis shows the goodness of fit for each of the solutions tested, with the vertical axis showing the lifetime, and the x-axis the maximum eccentricity of the planetary orbits. The upper plots show the results for solutions within 3 $\sigma$ of the best fit, whilst the lower show only those simulations within 1 $\sigma$ of that solution. Animated versions of the figures are provided in the online version of the paper.